Solid Freeform Fabrication 2017: Proceedings of the 28th Annual International Solid Freeform Fabrication Symposium – An Additive Manufacturing Conference
Reviewed Paper

INVESTIGATION OF OPTICAL COHERENCE TOMOGRAPHY IMAGING IN NYLON 12 POWDER

Adam Lewis[1], Nitesh Katta[2], Austin McElroy[2], Thomas Milner[2], Scott Fish[3], Joseph Beaman[3]

[1]McKetta Department of Chemical Engineering
[2]Department of Biomedical Engineering
[3]Department of Mechanical Engineering
Cockrell School of Engineering, The University of Texas at Austin, Austin, TX 78705

Abstract

Optical Coherence Tomography (OCT) has shown promise as a new process sensor in selective laser sintering (SLS) which can yield depth resolved data not attainable with conventional sensors. However, OCT images of nylon 12 SLS parts and powder contain artifacts, which have not been previously investigated in literature. These artifacts along with the highly scattering nature of the SLS parts and powder limit the imaging depth, which decreases the usefulness of OCT imaging. This study seeks to study the causes of the imaging artifacts and proposes and investigates methods to improve OCT imaging depth in nylon 12 powder.

Introduction

Selective Laser Sintering

Selective Laser Sintering (SLS) is one the earliest commercialized additive manufacturing technologies. SLS has found use in a wide swath of industries including aerospace and medical devices where, according to a recent report, it accounted for the largest share of the 3D printed medical devices market in 2016 [1]. This powder bed fusion process is able to produce parts with strengths comparable to injection-molded parts. A schematic demonstrating how the SLS process works is shown in Figure 1.

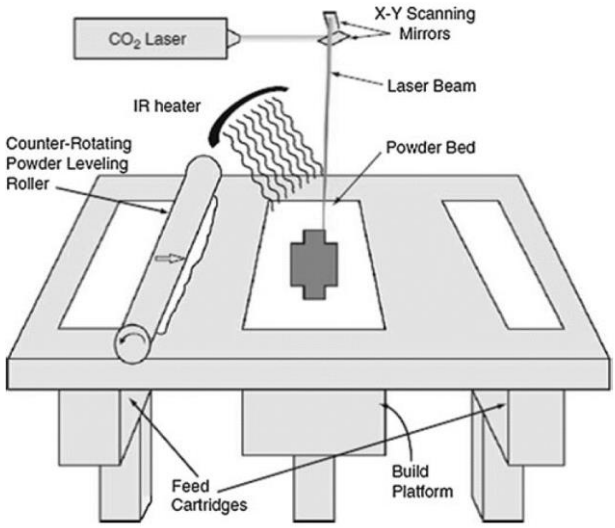

Figure 1. Selective Laser Sintering Schematic [2]

During the build process, while maintaining the top layer (typically around 100 microns thick) of polymer powder about 10°C below its melting point, a laser is used to melt select portions of the powder. Next, a new layer of powder is spread on top of the previous layer and the process is repeated until the part is completely formed. It is generally desirable to keep the entire melted material in a liquid state until the entire part can be cooled down as uniformly as possible in order to minimize thermal stresses and resulting warpage.

The powders used in the SLS process are typically semicrystalline with nylon 12 being the most common. As mentioned, the nylon 12 is a powder, melt, and solidified part at various times in the SLS build process. The crystallinity of the nylon varies in each of these phases as well. Various researchers have measured crystallinity values in nylon powder with values ranging from 45-51% [3]–[7]. These crystals are largely melted and portions of the powder become liquid during the build phase. Then, the nylon solidifies as it recrystallizes during cooling leaving a crystallinity in the cooled parts of around 21-31% depending on build conditions [3]–[8].

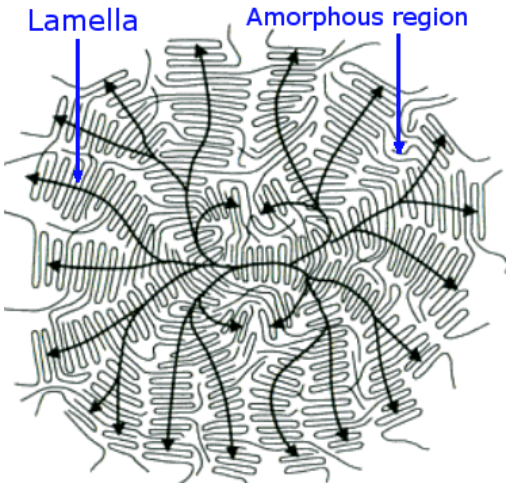

Figure 2. Schematic of a semicrystalline polymer spherulite [10]

The crystals in the solidified part grow spherically outward from the nucleation site and are known as spherulites. The degree of crystallinity of the parts and the size of such spherulites are affected by the cooling rate with faster cooling times resulting in a lower degree of crystallinity and smaller spherulites while slower cooling times result in a higher degree of crystallinity and larger spherulites [9]. The spherulites are semicrystalline meaning that the material is composed of both crystalline and amorphous regions as shown in Figure 2.

Despite the applications of SLS in various industries, it is common for SLS part properties to vary, even amongst different specimen contained within the same build. A desire to improve consistency of parts has led to an interest in improved process sensing and control in the SLS process. One of the technologies being investigated as an improved process sensor for SLS is Optical Coherence Tomography (OCT).

Optical Coherence Tomography

Optical coherence tomography (OCT) is an established medical imaging technique based on coherence interferometry commonly used in biomedical optics and medicine. In that application, OCT has the ability to provide real time subsurface visualization of human tissues at sub 10μm resolution. OCT data can be used to produce cross-sectional and volumetric images from magnitude and echo time delay data of backscattered radiation. A single OCT scan at a point on the surface of the sample is known as an A-scan and yields depth information at this point. A collection of subsequent A-scans is called a B-scan and yields a cross sectional image of the sample. Subsequent B-scans can be combined to yield a 3D representation of the sample as shown in Figure 3. The backscattered intensity information is typically presented in the false color of B-scans and volumetric renderings.

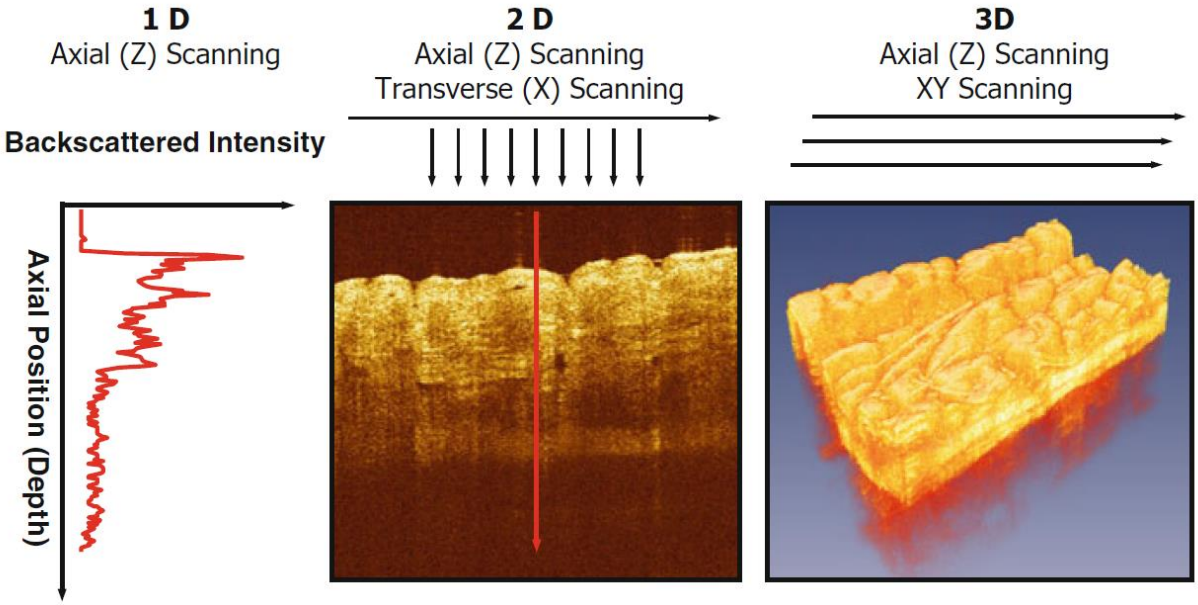

Figure 3. Typical OCT data visualization (Left) A-scan (Middle) B-scan (Right) Volumetric Rendering [11]

It is important to remember that each pixel in an A-scan is related to the amount of backscattered radiation collected at a certain time. This causes a millimeter of water to appear "thicker" than a millimeter of air in an OCT image because of the different speeds of light propagation in the different media given by their indices of refraction. This also means that when light scatters off multiple surfaces before being collected, it appears that the backscattering occurred lower in the B-scan image than it did physically.

Optical Coherence Tomography in Selective Laser Sintering

Research applying OCT to SLS is sparse. In 2015, Guan et al. reported having used OCT in SLS parts after being built to look at surface voids, surface roughness, and subsurface voids within a few layers of the surface [12]. It was recognized that adjacent areas of loose and sintered powder have different attenuation coefficients, and that the subsurface powder scatters more

strongly than sintered material. Therefore, in subsequent work [13], Guan et al. found a negative correlation between the number of pixels above a threshold intensity value in OCT B-scans of SLS parts and the sintering power used to sinter the part. The correlation was most clear at lower laser powers and dropped off at higher laser powers. They also identified purposefully under sintered powder beneath a single sintered layer through examination of the attenuation coefficient of the OCT signal. In 2016, Lewis et al. boresighted an OCT imaging laser with the sintering laser on an SLS machine in order to image during the SLS build process [14]. It was found that various layers could be simultaneously differentiated in the OCT images at low laser powers, potentially opening the way for interlayer bonding characterization. Additionally, a common defect known as part curl was able to be identified before causing an SLS build to fail.

Thus, OCT has been investigated as an ex-situ defect detection tool, but the OCT imaging depth of nylon parts has been found to be limited to a few hundred microns, reducing the usefulness of OCT in that application. Additionally, OCT has shown promise as an in-situ process sensor capable of providing subsurface information during the SLS build process, but the highly scattering nature of the nylon 12 parts and powder is not well understood. Furthering this understanding is valuable to progress both of the mentioned uses of OCT in SLS and is the aim of the present work.

Materials and Methods

Nylon Powder and Ethyl Cinnamate

All of the powder imaged in this paper was commercially available, virgin PA650 (nylon 12) from Advanced Laser Materials (ALM). The data sheet provided by ALM gives a particle size range, D10-D90, of 30 to 100 μm and a mean particle diameter of 55 μm. The melting temperature is reported at 181°C. Nylon powder was imaged in air as well as ethyl cinnamate. The ethyl cinnamate had a 99% assay, an index of refraction of 1.558, and was obtained from Sigma Aldrich [15].

OCT Systems

In this work, two different commercially available Fourier domain, swept source OCT systems were used which will be referred to as System A and System B.

System A comprised of a commercially available AXSUN swept source laser with details given in Table 1. The lateral resolution is given by the spot size, which was simulated to be 6μm. The axial pixel resolution was determined by moving the mirror in the sample arm. Using a precision micrometer (Z825B Thor Labs Inc.), the mirror interface was moved 1 millimeter to determine the change in the pixel value. This gave a per pixel movement of 3.75 μm/pixel. The lateral pixel resolution was determined by imaging a ruler and dividing 4mm by the number of pixels between the 4mm tick marks and was found to be 16 μm/pixel.

The axial (depth) resolution of OCT System A is defined as the smallest distance that can be discriminated at a refractive index discontinuity. To evaluate the axial (depth) resolution of the OCT system, the mirror's FWHM (Full Width Half Maximum) at the interface between air

and the mirror was utilized. The FWHM in pixels was about 1-2 pixels, hence the axial resolution of the system was determined to be about 5.6 ± 2μm.

Table 1: Key Parameters for OCT System A

Swept Source Laser Parameters			
Average Output Power	30 mW	Sweep Rate	100 kHz
Central Wavelength	1310 nm	Wavelength Tuning Range	125 nm
Resolution Parameters			
Axial Spatial Resolution	5.6±2 μm	Lateral Spatial Resolution	6 μm
Axial Pixel Resolution	3.75 μm/pixel	Lateral Pixel Resolution	16 μm/pixel

System B also comprised of a commercially available AXSUN swept source laser with details given in Table 2. System B also contained a nanosecond pulsed thulium fiber laser (Nufern, SUB-1337) which could be used to radiate a sample while imaging. The thulium fiber laser operated at a wavelength of 1940nm, with a maximum average power of 15W. It emitted 100ns duration pulses with a maximum pulse energy of 500μJ. The axial spatial and pixel resolutions as well as the lateral pixel resolution were determined similarly to System A; however, the lateral spatial resolution was determined experimentally as described below.

A custom in-house-designed fast detection scheme using an InGaAs (G12182-003K, Hamamatsu) detector was used to record the intensity profile of the focused OCT beam at the back focal plane of the 25mm focal length scanning lens (AR112-ZC-XWL-25-25, ISP Optics Inc.) via use of precision mechanical stages (ATS100-150-u-20p, Aerotech Inc.) and placing the detector just behind a 2 micron diameter pin hole (P2S, Thor Labs Inc.). The x,y,z-stages were positioned carefully to obtain the optimal spot of the highest intensity and the spot size was estimated along one axis by translating the pinhole using the precision mechanical stage. The recorded lateral beam profile gave a FWHM lateral resolution of 20±2μm when using a 4mm collimator. Using a similar procedure, the spot size of the thulium laser was found to be 34±2μm.

Table 2: Key Parameters for OCT System B

Swept Source Laser Parameters			
Average Output Power	30 mW	Sweep Rate	100 kHz
Central Wavelength	1310 nm	Wavelength Tuning Range	100 nm
Resolution Parameters			
Axial Spatial Resolution	12±4 μm	Lateral Spatial Resolution (with 4mm collimator)	20±2 μm
Axial Pixel Resolution	8.6 μm/pixel	Lateral Pixel Resolution	varied

Three collimators (RC04, RC08 and RC12, Thor Labs Inc.) were used with OCT system B with beam diameters of 4, 8, and 12 mm resulting in various spot sizes. The lateral resolution scales inversely with the collimator diameter used. Changing the collimated beam diameter necessarily changes the Rayleigh length of the beam. The 4, 8, and 12 mm collimators caused Rayleigh ranges of around 240, 60, and 27 μm respectively, which for the 8 and 12 mm collimators is less than the diameter of many of the powder particles. The small Rayleigh lengths

result in a limited range where the b-scans are not highly blurred, but useful observations were obtained despite this limitation.

Results/Discussion

The OCT Systems were used to image nylon powder in air and ethyl cinnamate. Nylon powder was also imaged while being sintered with the thulium laser. Each is discussed in the following sections.

Nylon Powder in Air with OCT System A

First, an empty dish was imaged. As can be seen in the top of Figure 4, the top and bottom surfaces of the empty dish are clearly visible. A similar, but separate dish was then filled with nylon powder in such a way as to achieve a powder layer of varying thickness in the dish. The powder was then imaged in an area with the least powder thickness. As can be seen in Figure 4, the top and bottom surfaces of the dish are visible only through a very thin layer of powder.

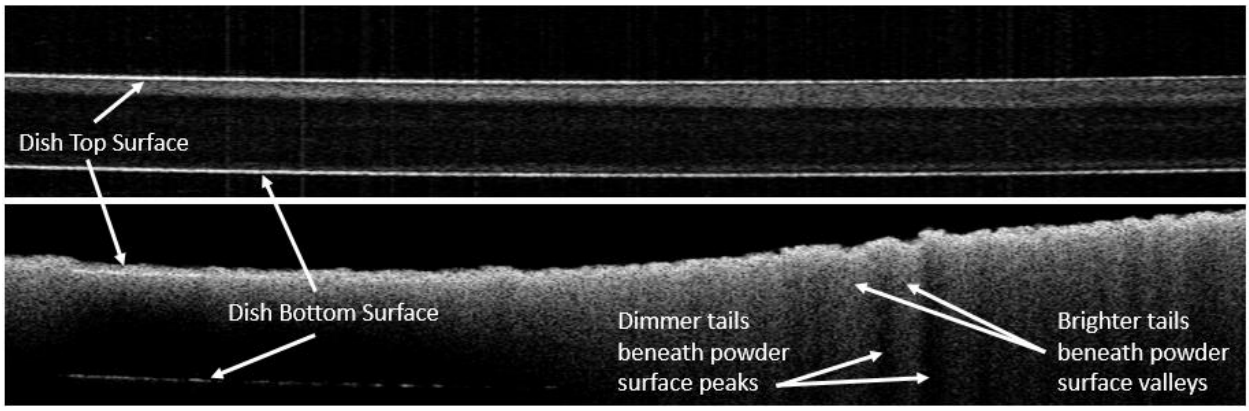

Figure 4. (Top) OCT Image of Empty Dish (Middle) OCT Image of Nylon Powder in Dish (Bottom) OCT Image of Nylon Dish with Dish and Powder Surfaces Marked

Additionally, a brightly reflecting region is visible beneath the powder that was not present in the image of the empty dish. Because these signal tails only occurred where the powder was present, it is likely that they were caused by multiple scattering events within and amongst the powder particles. It was also observed that signal tails beneath powder surface "valleys" were brighter than tails beneath powder "peaks." This also seems consistent with multiple scattering as a greater solid angle around a powder surface valley intersects with other powder particles than those around a powder surface peak as illustrated in Figure 5. A greater powder intersecting solid angle would mean a greater likelihood of a future scattering event, which could then contribute to the overall brightness of the signal tail.

To determine an indication of the height of powder through which imaging was possible, the visibility of the bottom of the plastic tray was used. First, a moving average filter was applied to each column of the powder dish imaging data. Then, imaging through the powder layer was defined to be possible if a pixel with an intensity above a predetermined threshold was present in the area where the bottom dish surface should appear.

To determine the powder thickness at a location, the powder surface location and the known dish thickness were subtracted from the bottom dish location. The powder surface location was assumed to be the first pixel in each column above a predetermined threshold and the dish thickness was determined from a part of the image containing no powder, and was assumed uniform.

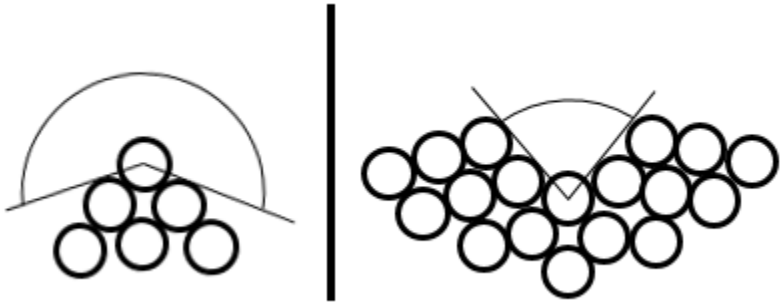

Figure 5. A Schematic of a raised powder particle (Left) and a sunken powder particle (Right) with the angle, which would not intersect nearby powder particles indicated. The powder intersecting angle is the conjugate of the angle shown here.

A histogram of the powder thicknesses through which imaging is possible is given in Figure 6. The index of refraction of the nylon powder was not measured, but is believed to be around 1.5 based on other polyamides [14]. In any case, a liberal imaging distance may be obtained by assuming a unity index of refraction. The histogram is dependent on the choice of threshold intensity values used during the analysis, but this does give some indication of the limited OCT imaging depth of nylon powder. Even using the liberal index of refraction, the mean penetration depth was less than the mean powder particle diameter.

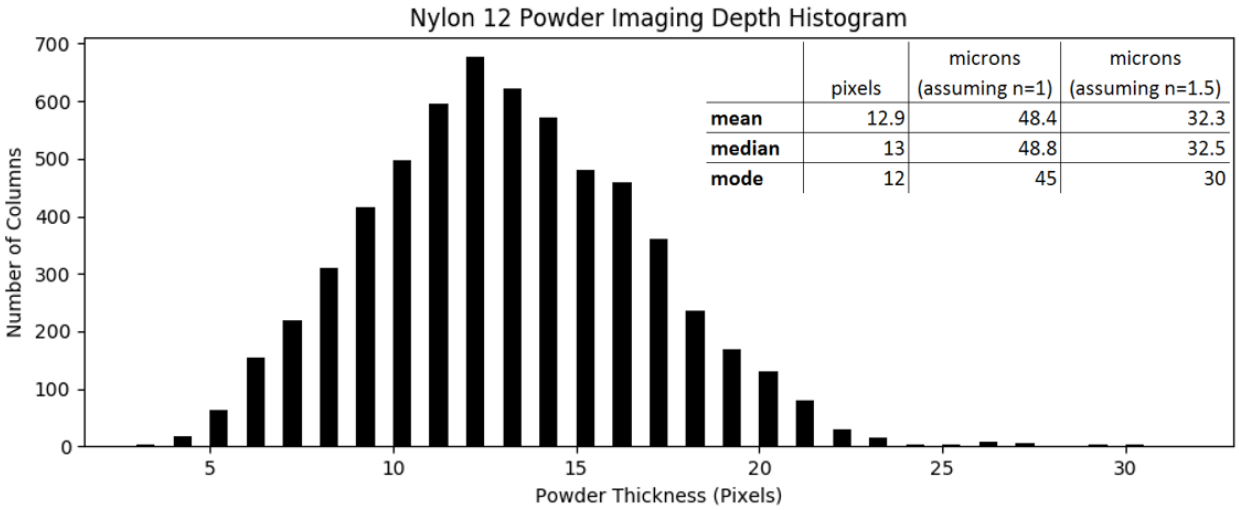

	pixels	microns (assuming n=1)	microns (assuming n=1.5)
mean	12.9	48.4	32.3
median	13	48.8	32.5
mode	12	45	30

Figure 6. A Histogram Showing the Powder Thickness through which OCT Imaging was Possible assuming various indices of refraction, n.

Individual Nylon Particles on Mirror with OCT System B

Individual PA650 particles were imaged on a mirror using OCT System B. Figure 7 shows an en face OCT image of three powder particles. The cross sectional view of the top particle is shown in the bottom three images using various intensity-to-grayscale maps in order to highlight certain features. In the bottom left image, only the highly reflecting mirror surface is visible. The mirror surface appears to curve beneath the powder particle due to the index of refraction mismatch of the powder and air. A signal tail starting at the particle and extending down below the mirror surface can be seen in the bottom right image. The tail is thought to be caused by total internal reflection of the OCT beam in the powder particle. The powder particle also appeared to be highly reflecting throughout the particle as opposed to scattering being limited to the air/particle interface. The authors hypothesize that the internal scattering events were due to the many scattering interfaces present in the spherulitic crystal structures of the powder particles.

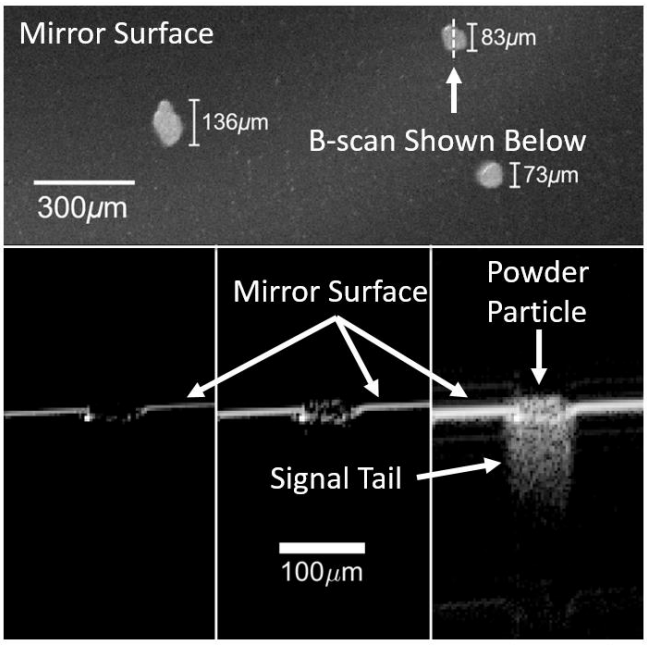

Figure 7 (Top) thing (Bottom Left) Thing (Bottom Center) Thing (Bottom Right)

Nylon Powder in Ethyl Cinnamate with OCT System B

Nylon particles were also imaged in ethyl cinnamate, which has an index of refraction of 1.558, nearly matching the suspected nylon 12 index of refraction of 1.5. By immersing the powder particles in a nearly index matching liquid, total internal reflection as well as multiple scattering events should be greatly reduced in the ethyl cinnamate/PA650 sample.

One hundred B-scans were averaged together to improve the signal to noise ratio. The resulting image is shown in Figure 8. It can be seen that the index-matched liquid eliminates the signal tail as expected. Now, the individual particles can be differentiated near the top as well as the liquid regions between the particles. Additionally, the imaging depth appears to be several hundred microns, an order of magnitude increase from imaging the particles in air. This indicates

that scattering rather than absorption is the limiting factor in imaging depth of nylon particles in air. Although not tested here, an index matching liquid could likely be used to increase the imaging depth of finished parts as well, provided the index matching liquid is able to be absorbed into the part.

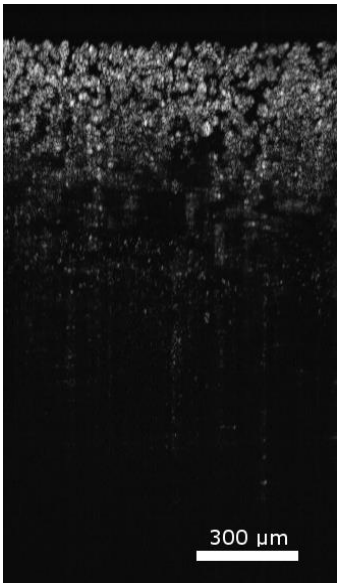

Figure 8. OCT Image of PA650 in ethyl cinnamate

Nylon Powder in Cuvette with Concurrent Sintering with OCT System B

Nylon powder was then imaged inside a cuvette while a portion of the nylon powder was melted from the side with a thulium laser as shown in Figure 9.

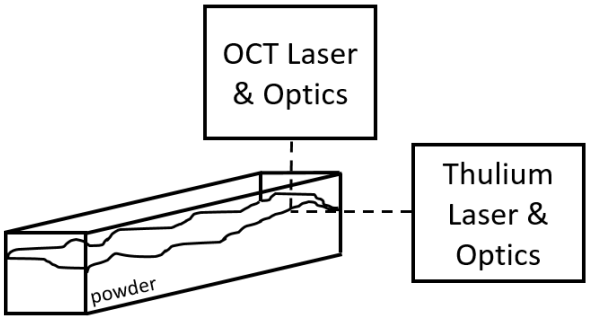

Figure 9. Schematic of setup for simultaneous imaging and melting of nylon 12 powder in a cuvette

The OCT laser began imaging after which the thulium laser was turned on for a fraction of a second and the OCT laser imaged for the next few seconds to capture the melting and resolidification of the nylon powder. Several of the captured images appear below in Figure 10.

Figure 10a shows the powder before the thulium laser was turned on. The powder surface appeared with a brightly reflecting surface and a signal tail as seen previously. Figure 10b shows the powder after the thulium laser began to heat the powder. The powder had shifted slightly, likely due to thermal expansion of powder below the surface, and the signal tail appeared to shimmer and shorten as the powder melted and became more transparent. Figure 10c shows the

agitating, transparent melt region. Several brightly reflecting powder particles were still visible. Figure 10d was captured a few seconds later after the transparent, melted region had stopped. Pores and perhaps some unmelted particles appeared to be present in the melted region. After this, Figure 10e shows the transparent region becoming more opaque starting from the surface of the melted region, and Figure 10f was taken after the opacity had stopped spreading.

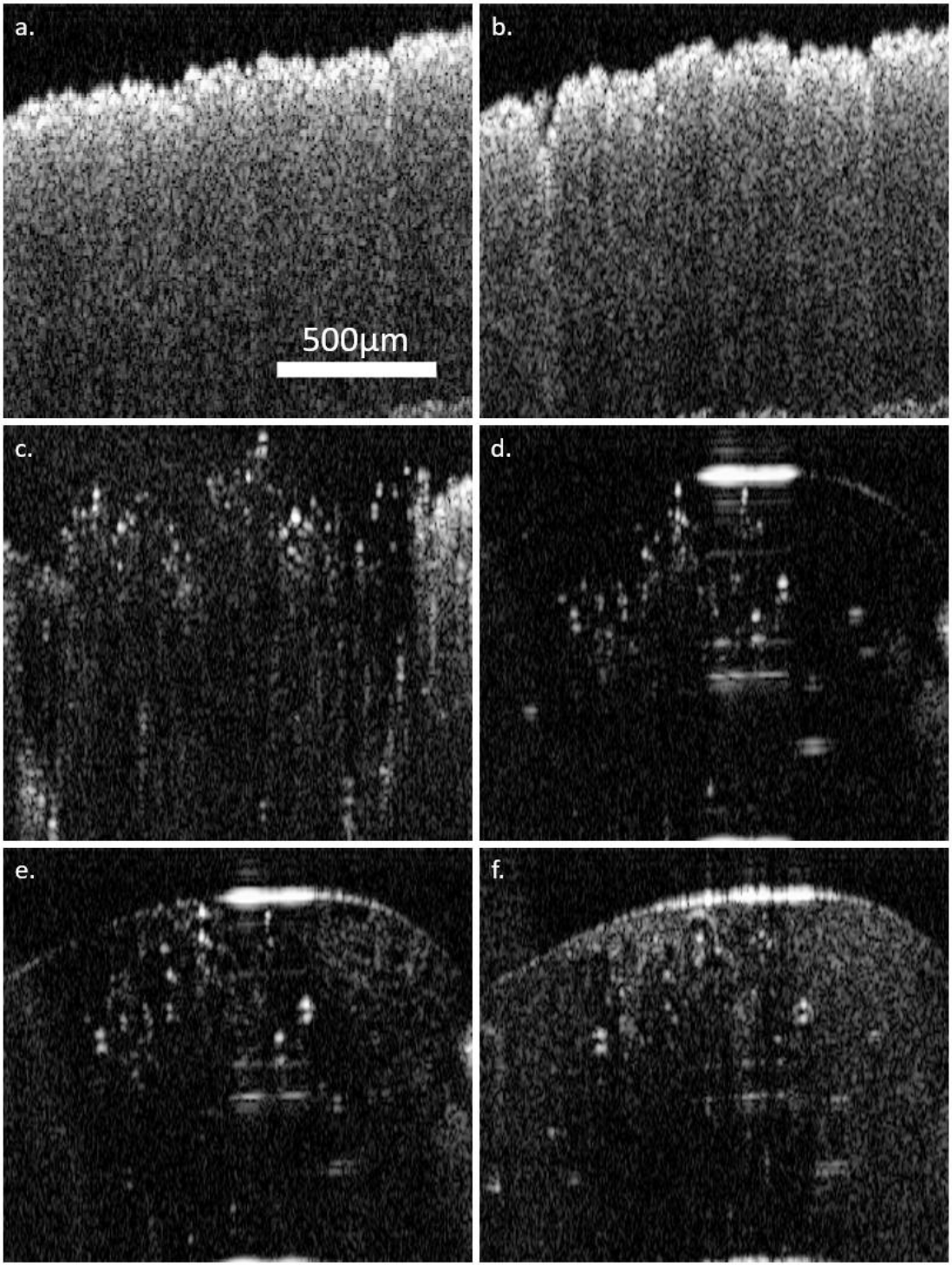

Figure 10. Nylon 12 powder at various stages of melting and resolidification

The authors hypothesize that the opacity seen in Figure 10e and Figure 10f was due to spherulite crystal growth as the melted region cools. This is consistent with opacity spreading from the surface of the melted region as it cooled since the surface of the melted region would reach the recrystallization temperatures first as the melted region cools. This is also consistent with the semicrystalline powder and sintered parts being highly scattering while the high temperature melted region was more transparent as was seen in this and other works [12]–[14].

Conclusions

In this paper it has been shown that the OCT imaging depth of nylon powder in air is limited to less than 100 μm. Evidence has also been presented which suggests that the limitation is due to both multiple scattering and total internal reflection. Additionally, the imaging depth of nylon powder was increased by an order of magnitude when immersed in an index matching liquid, which eliminated multiple scattering between the powder particles as well as the total internal reflection. Evidence has also been given which suggests that the crystal spherulites are responsible for much of the scattering in nylon 12. This would explain why the nylon melt appears transparent while nylon parts and powders are much more opaque in OCT images.

Acknowledgements

The authors would like to acknowledge the instrumental research support of the Air Force Research Lab (AFRL); General Dynamics Information Technology, Inc. (GDIT) PO# 08ESM753983: Laser Additive Manufacturing - Pilot Scale System (LAMPS) (PI: Scott Fish); the Office of Naval Research (ONR) Award# N00014-12-1-0811/N00014-16-1-2393: Physics and Cyber-Enabled Manufacturing Process Control for Direct Digital Manufacture of Metal Parts (PI: Joseph Beaman); and the National Science Foundation (NSF) Award # CNS-1239343: CPS: Synergy: Cyber Enabled Manufacturing Systems for Small Lot Manufacture (PI: Joseph Beaman) for their support of this research.

References

[1] "3D Printing Medical Devices Market by Component, Technology, Application,and End User - Global Industry Analysis and Forecast to 2025." [Online]. Available: http://www.marketresearchglobe.com/report/3d-printing-medical-devices-market-by-component-technology-applicationand-end-user-global-industry-analysis-and-forecast-to-2025. [Accessed: 27-Jun-2017].

[2] I. Gibson, D. W. Rosen, and B. Stucker, *Additive Manufacturing Technologies : Rapid Prototyping to Direct Digital Manufacturing*. Boston: Springer, 2009.

[3] H. Zarringhalam, N. Hopkinson, N. F. Kamperman, and J. J. de Vlieger, "Effects of processing on microstructure and properties of SLS Nylon 12," *Mater. Sci. Eng. A*, vol. 435–436, pp. 172–180, Nov. 2006.

[4] N. Hopkinson, C. E. Majewski, and H. Zarringhalam, "Quantifying the degree of particle melt in Selective Laser Sintering®," *CIRP Ann. - Manuf. Technol.*, vol. 58, no. 1, pp. 197–200, 2009.

[5] C. E. Majewski, H. Zarringhalam, and N. Hopkinson, "Effects of Degree of Particle Melt and crystallinity in SLS Nylon-12 parts," in *Materials*, Austin, TX, 2008.

[6] B. Van Hooreweder, D. Moens, R. Boonen, J.-P. Kruth, and P. Sas, "On the difference in material structure and fatigue properties of nylon specimens produced by injection molding and selective laser sintering," *Polym. Test.*, vol. 32, no. 5, pp. 972–981, Aug. 2013.
[7] H. Zarringhalam, C. Majewski, and N. Hopkinson, "Degree of particle melt in Nylon-12 selective laser-sintered parts," *Rapid Prototyp. J.*, vol. 15, no. 2, pp. 126–132, 2009.
[8] "Ajoku UK (2008) Investigating the Compression Properties of Selective Laser Sintered Nylon-12, PhD Thesis, Loughborough University. - Google Search." [Online]. Available: https://www.google.com/search?q=Ajoku+UK+(2008)+Investigating+the+Compression+Properties+of+Selective+Laser+Sintered+Nylon-12%2C+PhD+Thesis%2C+Loughborough+University.&oq=Ajoku+UK+(2008)+Investigating+the+Compression+Properties+of+Selective+Laser+Sintered+Nylon-12%2C+PhD+Thesis%2C+Loughborough+University.&aqs=chrome..69i57.455j0j4&sourceid=chrome&ie=UTF-8. [Accessed: 15-Dec-2016].
[9] S. Kalpakjian and S. R. Schmid, *Manufacturing engineering and technology*, Seventh edition. Upper Saddle River, NJ: Pearson, 2014.
[10] *By Materialscientist (Own work (transfer my upload from en.wiki)) [CC BY-SA 3.0 (http://creativecommons.org/licenses/by-sa/3.0) or GFDL (http://www.gnu.org/copyleft/fdl.html)], via Wikimedia Commons*. .
[11] W. Drexler and J. G. Fujimoto, *Optical coherence tomography: technology and applications*, Second edition. Cham: SpringerReference, 2015.
[12] G. Guan *et al.*, "Evaluation of selective laser sintering processes by optical coherence tomography," *Mater. Des.*, vol. 88, pp. 837–846, Dec. 2015.
[13] G. Guan, M. Hirsch, W. P. Syam, R. K. Leach, Z. Huang, and A. T. Clare, "Loose powder detection and surface characterization in selective laser sintering via optical coherence tomography," *Proc R Soc A*, vol. 472, no. 2191, p. 20160201, Jul. 2016.
[14] A. Lewis, M. Gardner, A. McElroy, T. Milner, S. Fish, and J. Beaman, "In-Situ Process Monitoring and Ex-Situ Part Quality Assessment of Selective Laser Sintering Using Optical Coherence Tomography," in *Process Development*, Austin, TX, 2016.
[15] "Ethyl cinnamate 112372," *Sigma-Aldrich*. [Online]. Available: http://www.sigmaaldrich.com/catalog/product/aldrich/112372. [Accessed: 22-Jun-2017].
[16] "Nylon 12." [Online]. Available: http://polymerdatabase.com/polymers/nylon12.html. [Accessed: 20-Jun-2017].